ACS APPLIED MATERIALS & INTERFACES

Research Article

www.acsami.org

Electropolymerized Highly Photoconductive Thin Films of Cyclopalladated and Cycloplatinated Complexes

Andreea Ionescu,[†,‡] Raffaella Lento,[§] Teresa F. Mastropietro,[∥] Iolinda Aiello,[†,‡] Roberto Termine,[†,⊥] Attilio Golemme,[†,§,⊥] Mauro Ghedini,[†,‡,⊥] Nathalie Bellec,[#] Elena Pini,[▽] Isabella Rimoldi,[▽] and Nicolas Godbert*[,†,‡]

[†]Centro di Eccelenza CEMIF.CAL, LASCAMM CR-INSTM, Unità INSTM della Calabria, I-87036 Rende, CS, Italy

[‡]Dipartimento di Chimica e Tecnologie Chimiche, [§]Dipartimento di Fisica, [∥]Dipartimento di Ingegneria per l'Ambiente e il Territorio e Ingegneria Chimica, and [⊥]UOS Licryl istituto IMIP del CNR c/o Dipartimento di Fisica, Università della Calabria, I-87036 Rende, CS, Italy

[#]Institut des Sciences Chimiques de Rennes, UMR 6226 CNRS-Université de Rennes 1, Campus de Beaulieu, Bât 10A, 35042 Rennes Cedex, France

[▽]Dipartimento di Scienze Farmaceutiche − Sezione di Chimica Generale e Organica "A. Marchesini", Università di Milano, Via Venezian 21, 20133 Milano, Italy

Supporting Information

ABSTRACT: The complete characterization of novel electropolymerizable organometallic complexes is presented. These are newly synthesized cyclometalated complexes of general formula (PPy)M(O∧N)^n (H(PPy) = 2-phenylpyridine, M = Pd(II) or Pt(II), H(O∧N)^n = Schiff base). Polymeric thin films have been obtained from these complexes by electropolymerization of the triphenylamino group grafted onto the H(O∧N)^n ancillary ligand. The redox behavior and the photoconductivity of both of the monomers (PPy)M(O∧N)^n and the electropolymerized species have been investigated. The polymeric films of (PPy)M(O∧N)^n have shown a very significant enhancement of photoconductivity when compared to their monomeric amorphous counterparts. The high stability of the obtained films strongly suggests that electropolymerization of cyclometalated complexes represents a viable deposition technique of quality thin films with improved photoconduction properties, hence opening the door to a new class of materials with suitable properties for optoelectronic applications.

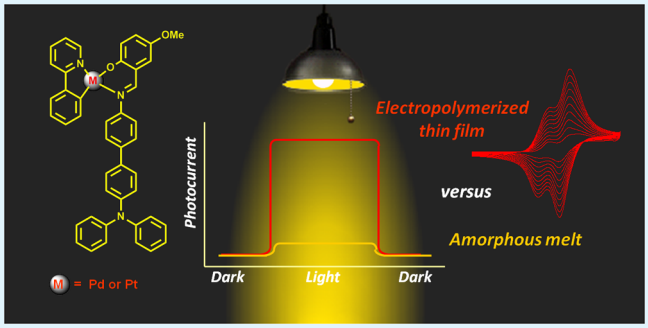

KEYWORDS: *palladium(II) complexes, electropolymerization, photoconductivity*

1. INTRODUCTION

Organic-based electronics have experienced in recent years impressive progress due to the development of novel organic semiconductors.[1−5] By introducing processability enhancing functionalities into their chemical structure, semiconducting materials can be applied in different fields, including thin film transistors, sensors, photodetectors, lasers, electroluminescent, and photovoltaic devices.[6] Semiconductors where charge carriers are generated in situ upon light absorption are called photoconductors.[7] The photoconduction process starts with the photogeneration of charges (extrinsically or intrinsically),[8,9] followed by the charge transport throughout the semiconducting material. The limited photogeneration efficiency represents the main drawback in the use of organic photoconductors.[10,11] To overcome this issue, the introduction of metal centers has demonstrated to be an appealing strategy because it can lead to the formation of organometallic complexes showing efficient charge generation features. To this regard, a series of photoconductive square planar Pd(II) and Pt(II) complexes were recently reported by our group.[12−15] These complexes, featuring a five-membered Pd(II) or Pt(II) metallacycle, formed by a (C∧N) cyclometalated ligand such as 2-phenylpyridine H(PPy), azobenzene H(Az), or benzo[h]-quinoline H(Bq) and a six-membered metallacycle obtained upon deprotonation of a Schiff base H(O∧ N) ancillary ligand (Figure 1), have shown excellent photorefractive properties both in their amorphous phases[16] and dispersed in a polymeric matrix.[17,18] The enhanced efficiency of photogeneration in these cyclometalated complexes is attributed, as revealed by theoretical studies, to the favorable combination of features such as (i) the square planar metal coordination geometry; (ii) the HOMO−LUMO separation in space on a molecular scale with the LUMO orbital predominantly situated onto the cyclometalated ligand and the HOMO onto the Schiff base

Received: October 13, 2014
Accepted: January 23, 2015
Published: January 23, 2015

DOI: 10.1021/am506984m
ACS Appl. Mater. Interfaces 2015, 7, 4019−4028

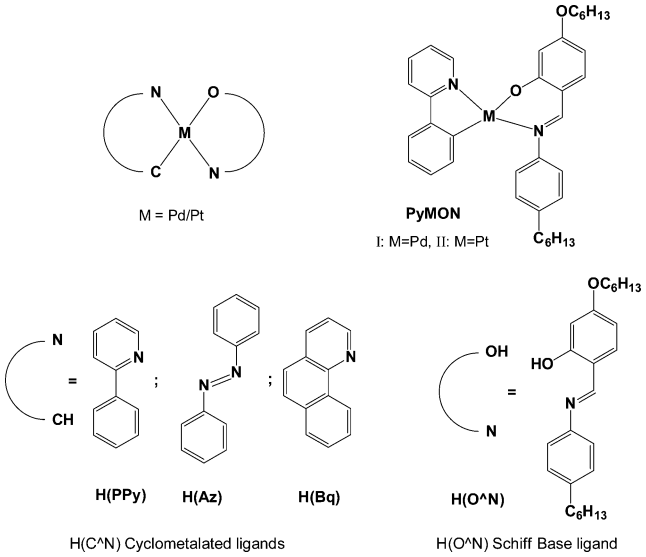

Figure 1. Photoconductive cyclometalated complexes.

ancillary ligand; and (iii) a conformational rearrangement upon excitation, slowing charge recombination.[13]

A possible route for increasing the photoconductive properties of these materials and facilitate their insertion into optoelectronic devices could be based on thin film processing such as derived from polymerized materials. To this regard, electropolymerization features several advantages over different solution-based film generating techniques usually employed for transition metal complexes.[19] By electropolymerization, the polymer formation and its deposition occur simultaneously, avoiding solubility drawbacks and affording controllable film composition, thickness, and homogeneous surface coverage. Since the early Abruna et al.[20] report on the reductive electropolymerization of vinyl-substituted polypyridine complexes, different electropolymerizable groups such as thiophene,[21−24] pyrrole,[25] aromatic amine,[26−28] and triphenylamino[29−31] fragments have been introduced into organometallic compounds. In this context, an organoplatinated electropolymerizable complex bearing a substituted arylamine fragment was recently reported, and the obtained electrogenerated thin film showed electrochromic behavior.[32]

We present herein the synthesis and characterization of a series of novel electropolymerizable photoconductive organometallic Pd(II) and Pt(II) complexes **1−6** (Chart 1) and the investigation of the properties of the corresponding polymeric films obtained by oxidative polymerization of a grafted triphenylamino group (TPA). The choice of the triphenylamine fragment as an electropolymerizable group has been motivated by (i) the formation of a cross-linked highly conjugated polymeric network, favoring isotropic charge transport through the material;[33] (ii) the use of a donor moiety with high hole transport properties;[34] situated onto the HOMO-holder ancillary ligand for improved charge separation; and (iii) the high electrochemical stability of the potential resulting polymer such as usually encountered for TPA-based electropolymers.[29−31]

A complete electrochemical study has been performed on both the monomers and the electropolymerized organometallic species. Furthermore, the photoconductive properties of amorphous and polymeric films obtained from the cyclometalated complexes have been investigated.

Chart 1. Molecular Structures of Complexes 1−6

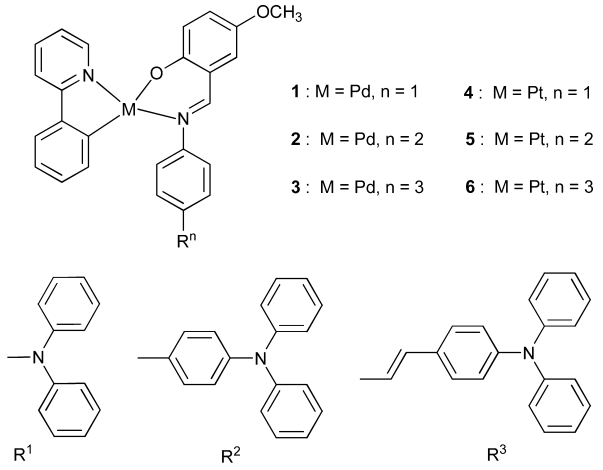

2. RESULTS AND DISCUSSION

A 2-phenylpyridine fragment has been chosen as an archetype cyclometalated ligand as in the parent photoconductive PyMON complexes[13] **I** and **II** (Figure 1), while the metal (Pd(II) or Pt(II)) coordination sphere of the novel complexes **1−6** (Chart 1) has been completed by three different triphenylamino-substituted potentially electropolymerizable Schiff bases H(O∧N)^n, n = 1−3. The choice of these specific ancillary ligands was directed by the wish to evaluate the influence of the physical distancing of the triphenylamine donor fragment from the photogenerating core, with the expectation to further stabilize the photogenerated exciton, hence further boosting the photogeneration efficiency.

Synthetic Procedure. The synthesis of complexes **1−6** (Scheme 1) was achieved in two steps. Pd(II) complexes **1−3** were synthesized through the formation of their corresponding cyclopalladated acetato bridged binuclear intermediate **A** obtained by cyclometalation of the H(PPy) ligand with palladium acetate.[35] Pt(II) complexes **4−6** were obtained instead from a cycloplatinated mononuclear intermediate

Scheme 1. Synthesis Pathway to Complexes 1−6[a]

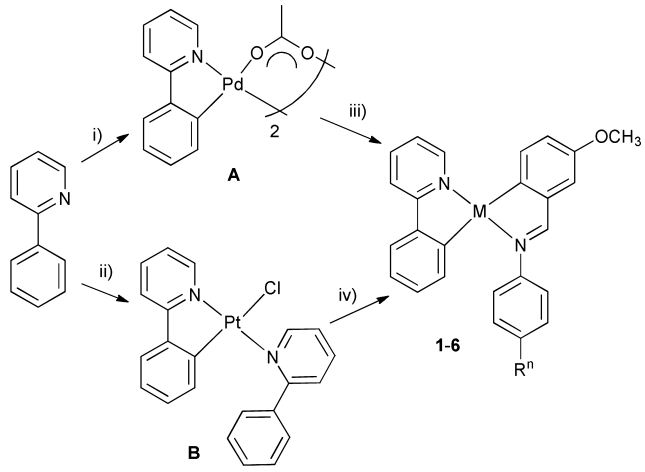

[a]Reagents and conditions: (i) $Pd(CH_3COO)_2$, CH_3COOH, 50 °C, 3.5 h; (ii) K_2PtCl_4, 2-$CH_3CH_2OCH_2CH_2OH$:H_2O, 3:1 (v:v), microwave irradiation (3 cycles, 2 min, 65 °C, 250 W); (iii) H(O∧N)^n, CH_3CH_2OH, rt, 24 h; (iv) H(O∧N)^n, 2-$CH_3CH_2OCH_2CH_2OH$, Na_2CO_3, 80 °C, overnight.

DOI: 10.1021/am506984m
ACS Appl. Mater. Interfaces 2015, 7, 4019−4028

complex **B** synthesized through microwave-assisted synthesis as previously reported.[36] The bridge cleavage of **A** and the substitution of **B** with the Schiff bases H(O∧N)^n, n = 1−3, afforded the final complexes in good yields. The Schiff bases were obtained by condensation of 5-methoxy-2-hydroxybenzaldehyde with an opportunely substituted triphenylamino derivative (see the Supporting Information).

X-ray Diffraction Studies. Single crystals of **1**−**5** suitable for X-ray structural determination were obtained from the slow evaporation at room temperature of a dichloromethane−ethanol (50% v/v) solution of the compounds. Unfortunately, it was not possible to obtain crystals of suitable quality in the case of **6**. All compounds produced yellow-orange spatula-shaped crystals featuring a rubber-like consistency (Figure 2).

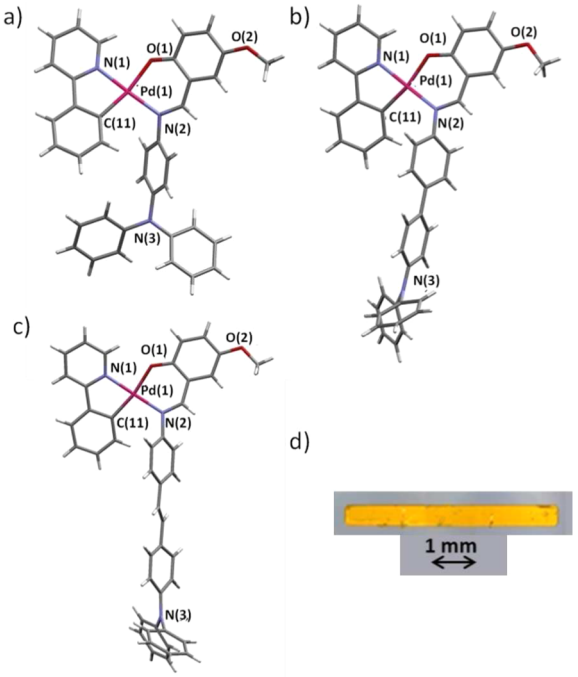

Figure 2. View of a molecular unit in compounds **1** (a), **2** (b), and **3** (c) and the atomic numbering scheme. For clarity, only one set of phenyl rings is shown for the disordered diphenylamine group in **3**. A picture (d) of a typical single crystal of **3**.

Crystals were flexible enough to be easily bent causing no breaking, while it was rather tricky to neatly cut them. When cut, all crystals revealed a fibrous "straw-like" texture.

As expected, **1** and its Pt(II) clone **4** are isostructural and crystallize in the monoclinic $P2_1/c$ space group. The asymmetric unit of both compounds is made up of a single metal complex, containing either Pd(II) (**1**) or Pt(II) (**4**). On the contrary, **2** and **5** are not isostructural, most likely due to the presence of a cocrystallized molecule of dichloromethane in **5**. They crystallize in the triclinic $P\bar{1}$ and monoclinic $P2_1/n$ space groups, respectively. In both cases, the asymmetric unit is made up of two crystallographically independent metal complexes. The presence of two rotationally free phenyl rings on the Schiff base most likely accounts for the differences in the molecular conformation observed in the two complexes, in turn resulting in the breaking of the symmetry. Compound **3** crystallizes in the triclinic $P\bar{1}$ space group, and the asymmetric unit consists of one Pd(II) metal complex. A molecular complex is shown in Figure 2 for **1** (a), **2** (b), and **3** (c), respectively.

In all compounds, the (C∧N) cyclometalated PPy ligand and the triphenylamino substituted (O∧N) Schiff base ligand coordinate the M(II) metal centers in a slightly distorted square planar geometry and in a *N,N* trans configuration. In all compounds, the larger deviation from the ideal square planar geometry was observed for the nitrogen atom of the PPy ligand, with calculated distances from the coordination mean plane falling in the range from 0.07(1) (**3**) to 0.10(1) Å (**1** and **4**). The bond distances and angles of the (C∧N)M(O∧N) chromophore are comparable to those observed in other similar compounds.[13] Crystal data, structure refinement, and selected bond angles and distances for **1**−**5** are reported in the Supporting Information (Tables S1 and S2).

While the (C∧N) five-membered ring resulting from the cyclometalation of the PPy ligand is almost planar in all of the complexes, the (O∧N) six-membered ring, formed by the chelation to the metal ion of the Schiff base ligand, features a severe deviation from planarity, the larger deviation being observed in one of the complexes of **5**. In particular, the Schiff base ligand is somewhat tilted with respect to the metal coordination plane, as shown in Figure 3. The dihedral angle

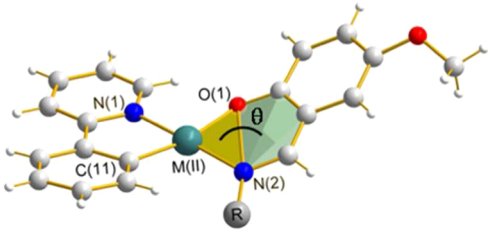

Figure 3. View of the tilting of the Schiff base with respect to the coordination plane defined at the metal center.

between the best mean plane calculated for the N(2)CCCO(1) set of atoms and the plane defined by the N(2)MO(1) set of atoms (180° − θ, Figure 3) is ca. 22° (**1**), 17° (**3**), and 21° (**4**). In complexes **2** and **5**, the corresponding values are ca. 11° (**2**) and 32° (**5**) at Pd(1) and 9° (**2**) and 4° (**5**) at Pd(2). The fluctuation in values of this dihedral angle demonstrates the high flexibility of the coordination of the Schiff base ancillary ligand.

The rotationally free phenyl rings directly linked to the Schiff base are tilted around the C−N bond with respect to the metal coordination plane, with dihedral angles between the best mean planes of ca. 66°, 68°, and 60° in **1**, **3**, and **4**, respectively. Similar values are found in **2** and **5**, even if differences in the orientation of the phenyl rings can be observed when comparing the two molecular complexes constituting the asymmetric unit (dihedral angles of ca. 66° and 60° for the Pd(1) and the Pd(2) complexes, respectively, in **2**, and ca. 67° for Pt(1) and 64° for Pt(2) complexes in **5**). Moreover, in **2** and **5** the two adjacent phenyl rings on the ancillary ligand are not coplanar, the degree of tilting defined as the torsion angle around the C−N bond being 26.2(3)° and 21.6(3)° in the Pd(1) and Pd(2) molecules, respectively, in **2**. The corresponding values are 35.6(1)° and 25.0(1)° in **5**.

With the sole exception of **5**, compounds **1**−**4** show a similar supramolecular organization in the solid crystalline state, mainly resulting from the mutual segregation of the triphenylamino moieties on the Schiff base and the cyclometalated cores. An

DOI: 10.1021/am506984m
ACS Appl. Mater. Interfaces 2015, 7, 4019−4028

example of the resultant layered structure is shown in Figure 4 for **1**. This layered architecture produced by the triphenylamine fragments can be correlated to the fibrous-like texture observed in the single crystals.

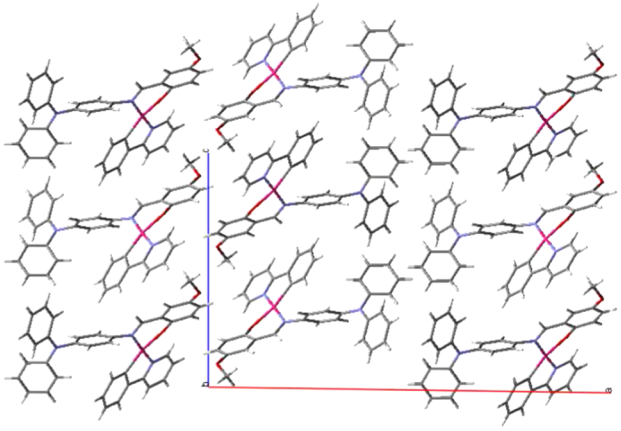

Figure 4. View of the crystal packing in **1**.

The crystal packing of **5** in the solid state shows instead tetranuclear supramolecular motifs assembled around the solvent molecules (Figure S2, Supporting Information).

Electrochemistry. The solution electrochemical data for complexes **1**−**6** were obtained by cyclic voltammetry, and the estimated HOMO energy values were determined. Data are collected in Table 1.

Table 1. Cyclic Voltammetry Data

complex	E^{ox}_1 (V)[a]	E^{ox}_2 (V)[a]	HOMO (eV)
1	+0.30 (Rev)	+0.59 (Rev)	−5.1
2	+0.34 (Irr)	+0.52 (Rev)	−5.2
3	+0.31 (QRev)	+0.48 (QRev)	−5.1
4	+0.37 (Rev)	+0.57 (Rev)	−5.1
5	+0.35 (Rev)	+0.51 (Rev)	−5.2
6	+0.32 (Rev)	+0.42 (Irr)	−5.1

[a]Potentials are given versus ferrocene/ferrocinium (Fc/Fc^+). Rev, reversible wave; QRev, quasi-reversible wave; Irr, irreversible wave. Measures performed in dichloromethane at 100 mV/s scan rate. $E^{ox} = (E^{pa} + E^{pc})/2$ for Rev and Irr processes, $E^{ox} = E^{pa}$ for Irr processes.

Two one-electron successive oxidation waves were observed for all complexes **1**−**6** with features characteristic of the triphenylamino fragment placed onto the Schiff base ligands.[37]

Noteworthy, both the nature of the metal (Pd(II) vs Pt(II)) and the distancing of the triphenylamino fragment from the metal center do not have a significant influence on the oxidation potentials; consequently, the HOMO values are similar for all of the compounds situated in energy at ca. −5.1 eV. Upon repetitive oxidation scans for all complexes **1**−**6** (0−1.4 V vs Ag wire pseudoreference electrode), a significant and constant increase in current is observed. Such behavior is typical of the electropolymerization of the substituted triphenylamino fragment.[29−31] The cyclic voltammogram of the electropolymerization process obtained for complex **1** is reported in Figure 5 as an example.

For all complexes, the modified Pt disk working electrode was immersed in a freshly distilled 0.1 M electrolytic dichloromethane solution, and a cyclic voltammogram was

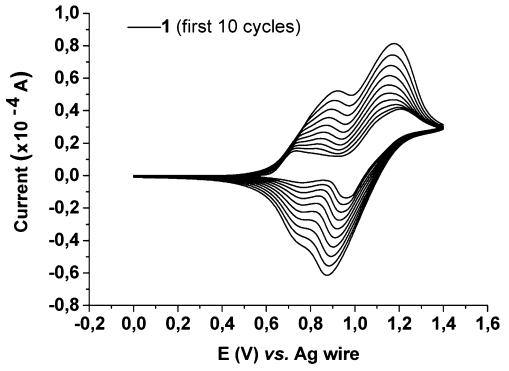

Figure 5. Cyclic voltammogram of **1** on a Pt disk working electrode in dichloromethane obtained upon 10 repetitive scans (0−1.4 V) at a scan rate of 100 mV/s.

recorded. The presence of a complete reversible oxidation process characterized by two consecutive oxidation waves and observed for all films generated from complexes **1**−**6** is indicative of the effective electropolymerization of thin films onto the Pt electrode surface. A typical cyclic voltammogram of a modified Pt electrode obtained from complex **1** is presented in Figure 6. The voltammograms related to complexes **2**−**6** are shown in the Supporting Information (Figure S1).

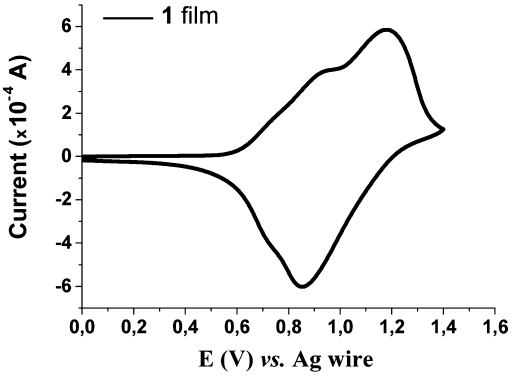

Figure 6. Cyclic voltammogram of a Pt disk-modified electrode in dichloromethane obtained after electopolymerization of **1**.

No reduction wave was recorded in the solvent window investigated (dichloromethane, −1.2 to +1.7 V) for all complexes **1**−**6**. Indeed, considering the HOMO/LUMO separation on a molecular scale identified for this class of Pd(II)/Pt(II) complexes,[13] the reduction process should be associated with the cyclometalated (PPy) ligand, whose reported reduction potential falls outside the potential window: for **I** and **II** (Figure 1) in DMF, E^{red} = −2.426 V and respectively E^{red} = −2.394 V.[13]

Although all complexes **1**−**6** do electropolymerize, to investigate the electrodeposition onto ITO covered glass and study the electrochemical properties of the obtained thin films, Pd(II) complex **2** and its corresponding Pt(II) analogue **5** were chosen as examples. Films of polymers derived from both complexes were electrodeposited on covered ITO-glass substrates from electrolytic dichloromethane solutions of 5.10^{-4} M of complex. The oxidative electropolymerization was achieved by continuously cycling the applied potential on the two consecutive redox processes. Cyclic voltammograms

DOI: 10.1021/am506984m
ACS Appl. Mater. Interfaces 2015, 7, 4019−4028

acquired during the electropolymerization processes at 100 mV/s scan rate are illustrated in Figure 7 for both complexes.

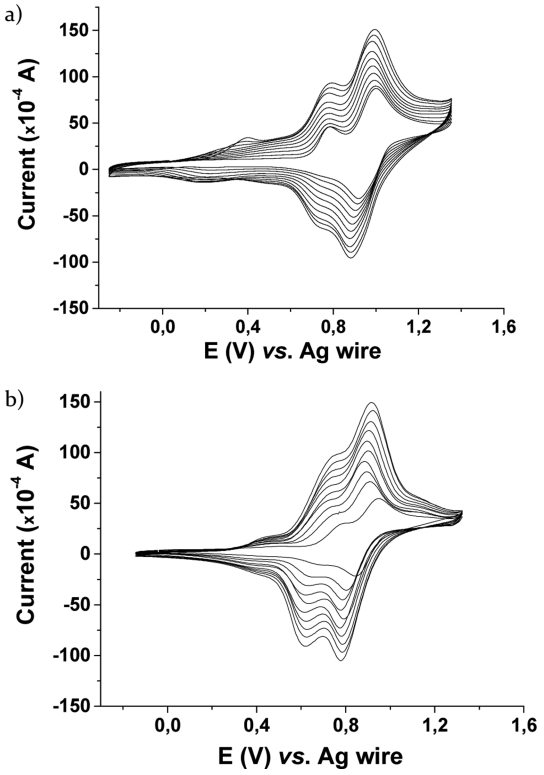

Figure 7. Electropolymerization of complexes **2** (a) and **5** (b) on ITO covered glass substrates in dichloromethane (note that plots are shown every 5 cycles).

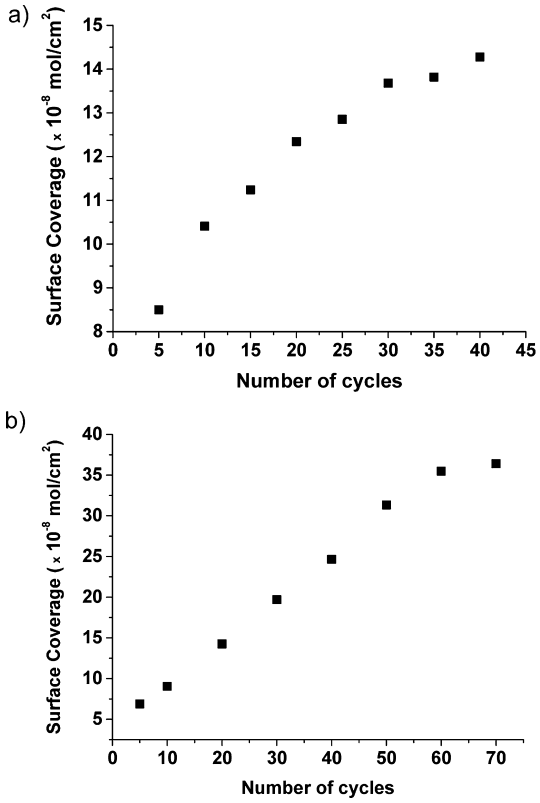

Figure 8. Profiles of surface coverage with the number of electropolymerization cycles. Data taken from the electrochemical characterization of films of complex **2** deposited on ITO covered glass of 2.25 cm^2 of surface area at 50 (a) and 100 mV/s (b) scan rates from a 5.10^{-4} M dichloromethane solution.

After electropolymerization, the resulting yellow films were aged overnight in a dichloromethane vapor saturated atmosphere before being washed with freshly distilled dichloromethane to remove unreacted monomer and adsorbed electrolyte. This particular aging step has shown to be highly effective to avoid films tearing and shrinking during the washing procedure.

Surface coverage of the ITO covered glass electrode, with respect to the number of cycles of electropolymerization, was determined through the equation: $\Gamma = Q/nFA$, where Γ is the surface coverage in mol/cm^2, Q is the charge in coulombs, A is the area of the electrode surface in cm^2, and n is the number of electrons transferred during the redox process.[38] Values of Q were determined by integrating the area under the cathodic peak during the characterization of the electrode in the supporting electrolyte solution. Surface coverage is strongly dependent on the scan rate as well as the reaching of a steady-state peak current during the electropolymerization process. Figure 8 shows the surface coverage obtained for complex **2** at 50 mV/s, for which a steady-state peak current is reached after approximatively 35 cycles, while at a scan rate of 100 mV/s, this steady state occurs only after 60 cycles.

As evidenced by the linear dependency of the peak currents versus the square root of the scan rate, diffusion-controlled conditions govern the mass transfer mechanism of the monomer to the electrode surface during electropolymerization. Figure 9 shows the anodic and cathodic peak currents at various scan rates during electopolymerization of both complexes **2** and **5** on a Pt disk working electrode.

Noteworthy, all electrodeposited thin films exhibit a stable cyclic voltammogram with no evidence of significant degradation after repetitive cycling on the two consecutive redox processes for several hundred cycles or after prolonged storage in air and also after maintaining the film at an oxidizing potential. The stability of 1 week-old films stored in air and exposed to light has been also tested in electrolytic solutions of acetonitrile and tetrahydrofuran. The films have shown stability for five consecutive cycles in these polar (nondry) solvents. These features show the high stability of the electropolymerized materials (see the Supporting Information for repetition cycling, Figure S5).

Film Morphology. The morphology of the electropolymerized thin films was investigated by AFM microscopy. Figure 10 shows a photograph of electrodeposited thin films of complex **5** on ITO covered glasses, obtained at various scan rates and showing the uniformity of deposition onto the surface electrode.

For high values of scan rate (ν > 100 mV/s), the surface morphology of the obtained thin films is relatively smooth with a root-mean-square roughness R_{RMS} of ca. 5 nm, as seen, for instance, in Figure 11a for complex **2** electrodeposited at a 250 mV/s scan rate. For lower scan rates, AFM images reveal a higher roughness of the film surface (R_{RMS} = 22 nm) and show a cauliflower-like texture similar in features to films of TPA obtained through solid-state electropolymerization[39] (Figure 11b).

Photoconductivity Measurements. Photoconductivity measurements were performed for complexes **1**, **2**, **3**, and **5**

DOI: 10.1021/am506984m
ACS Appl. Mater. Interfaces 2015, 7, 4019−4028

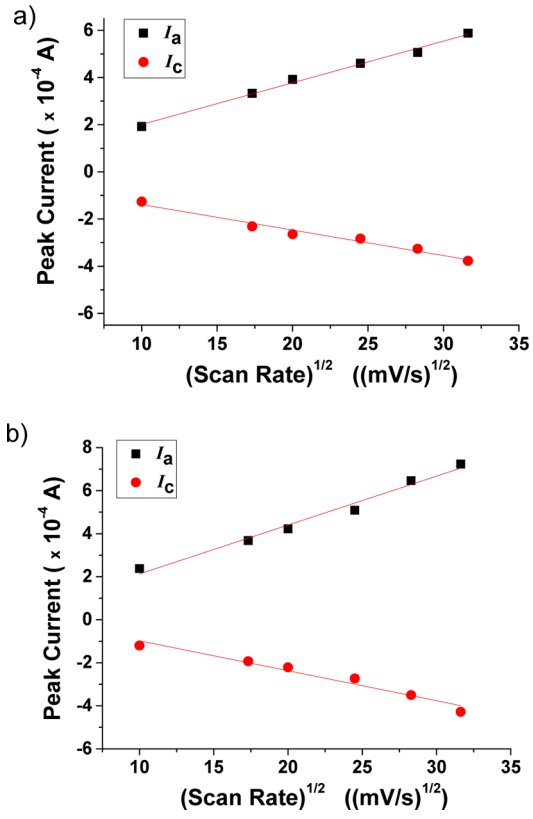

Figure 9. Plots of cathodic (I_c) and anodic (I_a) peak currents at various scan rates (100 mV/s to 1.0 V/s) for a 5.10^{-4} M complex solution in dichloromethane. Data taken during the 20th cycle of electropolymerization for the second redox process.

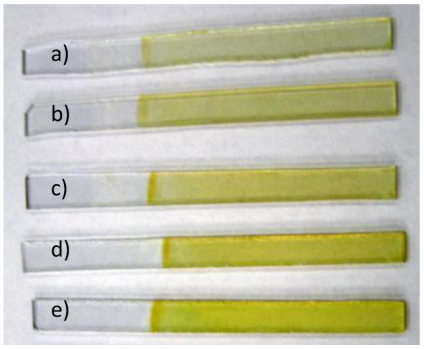

Figure 10. Photograph of electrodeposited thin films of complex **5** on ITO covered glass substrates, obtained from a 5.10^{-4} M dichloromethane solution, at different scan rate: (a) 1000, (b) 800, (c) 500, (d) 250, and (e) 100 mV/s.

in the amorphous state (see Experimental Section for details). Such measurements were not possible in the case of **4** and **6** due to the closeness between melting points and thermal decomposition temperatures, which prevented sample preparation (see the Supporting Information for DSC and TGA traces, Figure S3). The photoconductivity as a function of the applied field at λ = 532 nm is presented in Figure 12. Results for parent complexes **I** and **II** (Figure 1) recorded in identical conditions have been included for comparison. However, for these two reference complexes, measures were performed on crystalline samples[13] because it was not possible to reach, for these two complexes, an amorphous state upon cooling. For direct comparison among complexes, the photoconductivity has been

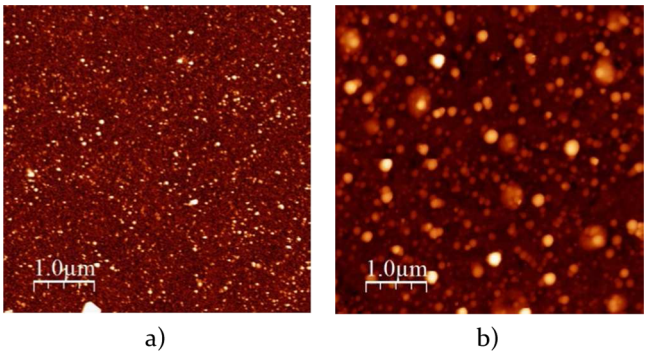

Figure 11. AFM micrographs of electrodeposited thin films of complex **2** on ITO covered glass substrates, obtained from a 5.10^{-4} M dichloromethane solution, at different scan rates: (a) 250 and (b) 50 mV/s.

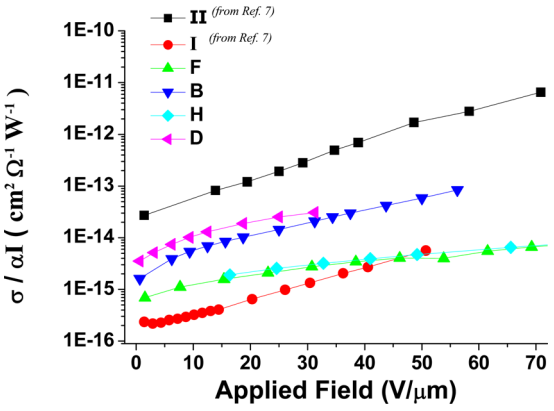

Figure 12. Normalized photoconductivity observed at λ = 532 nm for complexes **1**−**3**, **5**, **I**, and **II** as a function of the applied field.

normalized over the light intensity and the absorption coefficient α of each complex.

Photoconduction can be seen as the result of two distinct phenomena, photogeneration and charge transport. On one hand, the presence of the triphenylamino fragment onto the Schiff base ancillary ligand may increase the physical distance between the HOMO (mainly localized onto the triphenylamino fragment) and the LUMO (mainly localized onto the PPy cyclometalated ligand) when comparing complexes **1**−**6** with **I**,**II** analogues. On the other hand, the triphenylamino fragment is well-known for its donor properties and its good hole transport properties.[34] Finally, it is expected that in a more ordered and condensed physical state, the charge transport properties are exalted by a closer contact between neighboring molecules, and, consequently, crystalline samples may exhibit higher photoconductive response with respect to completely amorphous samples. In this light, it is not surprising that when compared to **I**, the new Pd(II) complexes **1**−**3** show photoconductivity responses of ca. 1 order of magnitude higher, even if they have been studied in their amorphous state, while for **I** a crystalline sample was used. As was previously observed for this class of complexes, the substitution of the Pd(II) metal center by Pt(II) results in an increase of photoconduction which may be correlated to the higher population of longer living excited triplet states in Pt(II) complexes.[13] However, this increase is less pronounced when passing from **2** to **5** than what is observed for the **I**/**II** couple (see Figure 12). This difference in behavior might be associated

DOI: 10.1021/am506984m
ACS Appl. Mater. Interfaces 2015, 7, 4019−4028

with the physical state of the samples (amorphous vs crystalline), which drastically affects the charge transport properties. **2** and **5** being amorphous samples, the beneficial effect of switching metal center is less pronounced. Similarly, due to this difference in the physical state of the samples, it is not surprising that all new complexes have shown photoconductive responses lower than that observed for the crystalline reference **II** sample, especially because the crystalline state of **II** is characterized by strong $\pi-\pi$ interactions of the ligands.[13]

A second feature of these measurements is the absence of correlation between photoconductivity and the physical distancing of the triphenylamino fragment from the metal center. Indeed, all Pd(II) complexes **1**−**3** present a quantitatively similar photoresponse, suggesting that both photogeneration and charge transport properties are similar for all Pd(II) complexes. Because there is no substantial difference in photoconductivity within both series of metal complexes, Pd(II) complex **2** and its Pt(II) counterpart **5** have been chosen as representative examples to investigate the effect of polymerization on the photoconductivity response of the materials.

Electropolymerized thin films of complexes **2** and **5** were deposited onto dedicated etched ITO covered glass substrates from electrolytic solutions of ca. 2.10^{-4} and 1.10^{-4} M for **2** and **5**, respectively, at 250 mV/s scan rate. After aging and washing following the previously mentioned procedure, the films thicknesses were measured using a stylus profilometer. Finally, the aluminum counter electrode (ca. 300 nm thick) was deposited onto the films by thermal evaporation at a base pressure of 10^{-6} mbar. Photoconduction measurements were performed by irradiating the samples in the absorption tail (λ = 532 nm) through the negatively polarized ITO-glass substrate. Photoresponses of the electropolymerized thin films are shown in Figure 13 together with those of their corresponding monomers in their amorphous states for direct comparison.

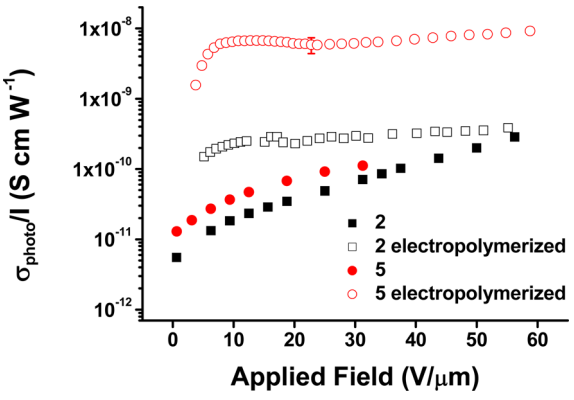

Figure 13. Photoconductive responses of complexes **2** and **5** and their corresponding electropolymerized thin films, 195 nm thick for **2** and 265 nm thick for **5**.

For both polymers, photoconductivity is 1 order of magnitude higher than dark conductivity. It should be underlined that, in both cases, the photoconductivity of the electrodeposited films is higher than that of the corresponding monomers. Furthermore, this difference is accentuated for low values of applied electric field. Considering that at low fields photogeneration efficiency increases rapidly with the electric field, while the increase of charge mobility is slower,[40,41] this behavior could be an indication that the photogeneration efficiency of the system increases with electropolymerization.

In addition, it has to be noticed that the thicknesses of the samples are rather different (ca. 4 μm for monomers vs ca. 200 nm for electropolymerized thin films) and that increased charge trapping might be present in thinner films due to the higher related impact of interfaces. For this reason, the photoconductivity values measured for the electropolymerized samples could even be underestimated. Further investigations are in progress to shed light on this issue.

The photoconductivity exhibited by the investigated polymers is several orders of magnitude lower than in silicon[42] or in amorphous inorganic materials.[43] This reflects the well-known fact that organic materials are characterized by lower charge mobility and photogeneration efficiency. At the same time, the possibility of comparison of the performance of the electropolymerized films presented in this work with the performance of state of the art organic photoconductors is limited by several factors. In fact, very often photoconduction data are reported without mentioning light intensity or as simple photocurrents. In addition, in contrast with the polymers studied here, organic semiconductors are often doped, to increase photogeneration efficiency. Moreover, to get more accurate data, in this work photoconduction was measured away from the maximum optical density, in the high wavelenth absorption tail (see the Supporting Information, Figure S4). Nonetheless, considering the best performing polymer, compound **5**, the photoresponse is orders of magnitude higher than in low molecular weight or polymeric materials, almost always doped, used as photorefractive media,[44,45] often based on poly(vinylcarbazole). The photoconductivity of **5** is of the same order of magnitude as in semiconducting polymers used to fabricate bulk heterojunction solar cells,[46] and only 2 orders of magnitude lower than in highly photoconducting doped polycrystalline organic films,[47] which were, however, handled and tested under vacuum and not in ambient conditions as in our case. Such excellent performance, together with the opportunities of easy and controlled patterning provided by the electropolymerization preparation method, paves the way toward the use of the polymers presented in this work in the development of optoelectronic devices.

3. CONCLUSION

A series of new photoconductive 2-phenylpyridine cyclometalated Pd(II) and Pt(II) complexes with a triphenylamino containing ancillary Schiff base ligand has been synthesized. By opportune synthetic methodologies, the distance between the metal center and the donor fragment has been incremented. Electrochemical data obtained for all complexes have confirmed the localization of the HOMO mainly onto the donor fragment. Upon repetitive cyclic voltammetry, an electropolymerization process has been evidenced for all complexes allowing the electrodeposition of homogeneous high quality photoconductive thin films. All complexes present photoconductivity in their amorphous state at λ = 532 nm. The photoresponse is independent of the position of the triphenylammine fragment. Electropolymerized thin films on ITO substrates have shown improved photoconductive behavior with respect to their corresponding monomers. Further investigations are in due course to correlate the photoconduction behavior with film thickness and morphology, both parameters being correlated and simultaneously dependent on the experimental conditions.

DOI: 10.1021/am506984m
ACS Appl. Mater. Interfaces 2015, 7, 4019−4028

These results confirm that electropolymerization of cyclometalated complexes can actually represent a useful procedure for the preparation of quality thin films for optoelectronic applications.

4. EXPERIMENTAL SECTION

Materials and Methods. All commercially available chemicals were purchased from Aldrich Chemical Co. and were used without further purification. IR spectra (KBr pellets) were recorded on a Spectrum One PerkinElmer FT-IR spectrometer. ^{1}H NMR spectra were recorded either on a Varian Mercury Plus 200 spectrometer or on a Bruker WH-300 spectrometer in deuterated solvents with TMS as internal standard. Elemental analyses were performed with a PerkinElmer 2400 analyzer CHNS/O. The thermal stability was measured on a PerkinElmer Thermogravimetric Analyzer Pyris 6 TGA, while phase transition temperatures and enthalpies were measured on a TA Instruments DSC Q2000 differential scanning calorimeter. Melting points were determined with a Leica DMLP polarizing microscope equipped with a Leica DFC280 camera and a CalCTec (Italy) heating stage. For AFM surface morphology characterization, samples were investigated using a NanoScope IIIa atomic force microscope (Veeco-Bruker) in tapping mode in air. For the measurements, silicon AFM cantilevers, with an elastic constant of 5 N/m (TAP150A, Bruker), were used.

Electrochemistry and Electropolymerization. All potentials were measured using an Epsilon electrochemical analyzer or on a Autolab potentiostat/galvanostat. Cyclic voltammetry experiments were performed in a 3 mL cell of dry, freshly distilled, and degassed (N_2) dichloromethane solution using tetrabutylammonium hexafluorophosphate (0.1 M) as supporting electrolyte, a Pt disk working electrode, a Pt wire counter-electrode, and an Ag wire as pseudoreference electrode. Voltammograms were registered at a 100 mV/s scan rate from a ca. 10^{-3} M complex solution. Redox potentials are given with respect to the ferrocene/ferrocenium (Fc/Fc^+) redox couple used as an internal reference. Estimation of HOMO/LUMO energy values was performed taking into account −4.8 eV for Fc/Fc^+.[48]

Electropolymerizations were carried out by cyclic voltammetry, performed with an Autolab PGSTAT 30 potentiostat/galvanostat controlled by the GPES v. 4.9 software. A conventional three-electrode cell was employed, with a Pt wire as counter-electrode, an Ag wire as pseudoreference electrode and a 2 mm wide ITO stripe on glass as working electrode. Tetrabutylammonium hexafluorophosphate (0.1 M) was used as supporting electrolyte, and experiments were performed in a dry, freshly distilled, and degassed (Ar) dichloromethane solution. The electropolymerization process was achieved by continuously cycling the applied potential around the oxidation potential of the studied complex at a constant scan rate. Films thicknesses (typically in the 200 nm range) were measured with a stylus profilometer (Veeco, Dektak 8). After electropolymerization, the resulting yellow films were aged overnight in a dichloromethane vapor saturated atmosphere before being washed with freshly distilled dichloromethane.

Photoconductivity Measurements. Suitably etched indium tin oxide (ITO) on glass substrates (VisionTek Systems Ltd., 12 Ω per square) were used to prepare the cells. Before being used, substrates were subsequently cleaned in an ultrasonic bath with acetone, NaOH (ca. 5%), distilled water, and finally isopropanol. The conducting ITO stripes were overlapped and assembled controlling the cell thickness by means of 1.7 μm spacers dispersed in thermal resistant glue. The real thickness of the cells was measured by recording the interferometric pattern in a UV−vis spectrophotometer. Cells were filled by capillarity at a temperature slightly above the melting point of the complexes. Rapid cooling to room temperature allowed the freezing of the melt into its amorphous thermostable state.

For electropolymerized devices, an Al layer (ca. 300 nm thick) was thermally evaporated on the previously deposited polymeric films, at a base pressure of 10^{-6} mbar, in a Kurt J. Lesker deposition chamber using a shadow mask. A solid-state laser (λ = 532 nm, Torus, Laser quantum) was used as the light source. The light intensity was $I \cong 1$ mW/cm^2, slightly different every time the setup was changed when switching samples. The photocurrent i_{photo} was obtained from the difference between light and dark currents ($i_{light} - i_{dark}$) measured with an electrometer (6517A, Keithley), also used to apply a potential difference on the electrodes.

X-ray Diffraction Studies. Selected crystals were mounted on a Bruker-Nonius X8APEXII CCD area detector system and used for data collection. Diffraction data were collected at room temperature by using graphite-monochromated Mo Kα radiation (λ = 0.71073 Å). The data were processed through the SAINT[49] reduction and SADABS[38] absorption software. Nevertheless, unsolved absorption effects, giving rise to high residual electron densities (3.69, 3.62, 3.60, and 3.54 e/Å^3) in the near proximity of the platinum metal center (distances in the range 1.26−2.58 Å), were observed in **3** during the final structure refinement. However, no unusual bond lengths and angles are observed, supporting the proposed model. The unit cell parameters are listed in Table 1 together with a summary of the structure refinement data. The structures were solved with the SHELX-NT software package[50] by standard direct methods and subsequently completed by Fourier recycling. All non-hydrogen atoms were refined anisotropically. The hydrogen atoms were placed in geometrically suitable positions and were refined as riding atoms. In **5**, the phenyl rings of the triphenylamine moiety on the ancillary ligand have been found disordered on two positions. Two different sets of carbon atoms have been defined from the Fourier map and refined with PART instruction, with a final occupancy factor of ca. 0.5. The final full-matrix least-squares refinements on F^2 reached convergence with values of the discrepancy indices given in Table 1. The final geometrical calculations and the graphical manipulations were performed using the XP utility of the SHELXTL system and the DIAMOND program.[51] Final refinement data for **1**−**5** are given in Table 1. Selected interatomic bond lengths and angles are given in Table S1 (Supporting Information). CCDC reference numbers are 1025751−1025755 for **1**−**5**, respectively. See http://pubs.acs.org for crystallographic data in CIF or other electronic format.

Synthesis. Pd(II) complexes **1**−**3** and their corresponding Pt(II) analogues **4**−**6** were prepared according to a typical procedure reported for **1** and **3**, respectively, as example preparations, while the syntheses of the Schiff bases $H(O\wedge N)^1$, $H(O\wedge N)^2$, and $H(O\wedge N)^3$ are fully described the in Supporting Information. The 2-phenylpyridine cyclopalladated binuclear intermediate **A** was obtained by cyclometalation of H(PPy) with palladium acetate as previously described,[35] while the mononuclear cycloplatinated intermediate **B** was obtained by microwave-assisted synthesis following the literature procedure.[36]

Synthesis of ***1****.* Intermediate binuclear complex **A** (100 mg, 0.156 mmol) and 2 equiv of $H(O\wedge N)^1$ (123 mg, 0.312 mmol) were solubilized in ethanol and stirred at room temperature for 24 h. The yellow precipitated solid was filtered off, washed with ethanol, and dried under vacuum. Recrystallization was performed in dichloromethane/ethanol solution.

1: orange solid; yield 80% (165 mg); mp 220 °C (amorphous on cooling); T_{dec} = 260 °C; ^{1}H NMR (300 MHz, $CDCl_3$, 25 °C, TMS) δ = 9.29 (dd, J = 6.6 Hz, J = 1.2 Hz, 1H), δ = 8.06 (s, 1H), δ = 7.82 (td, J = 8.2 Hz, J = 1.2 Hz, 1H), δ = 7.64 (d, J = 7.7 Hz, 1H), δ = 7.48 (d, J = 8.8 Hz, 1H), δ = 7.39 (d, J = 8.4 Hz, J = 1.5 Hz, 1H), δ = 7.3−7.2 (m, 4H), δ = 7.12−6.95 (m, 13H), δ = 6.81 (td, J = 6.2 Hz, J = 1.5 Hz, 1H), δ = 6.69 (d, J = 3.3 Hz, 1H), δ = 6.08 (dd, J = 13.8 Hz, J = 1.1 Hz, 1H), δ = 3.76 (s, 3H); FT-IR (KBr, cm^{-1}) 3041, 2993, 2923, 1620, 1586, 1452, 1438, 1414, 1383, 1319, 1290, 1273, 1214, 1154, 1039, 811, 755, 693. Anal. Calcd for $C_{37}H_{29}N_3O_2Pd$ (654.07 g/mol): C, 67.94; H, 4.47; N, 6.42. Found: C, 67.68; H, 4.45; N, 6.50.

Synthesis of ***2****.* Intermediate binuclear complex **A** (100 mg, 0.156 mmol) and 2 equiv of $H(O\wedge N)^2$ (147 mg, 0.312 mmol) were used.

2: orange solid; yield 94% (228 mg); mp 241−242 °C (amorphous on cooling); T_{dec} = 270 °C; ^{1}H NMR (300 MHz, $CDCl_3$, 25 °C, TMS): δ = 9.30 (dd, J = 5.7 Hz, J = 0.9 Hz, 1H), δ = 8.12 (s, 1H), δ = 7.82 (td, J = 8.1 Hz, J = 1.5 Hz, 1H), δ = 7.66−7.48 (m, 6H), δ = 7.36 (dd, J = 7.8 Hz, J = 1.5 Hz, 1H), δ = 7.31−7.22 (m, 5H), δ = 7.15 (m, 6H), δ = 7.07−7.02 (m, 4H), δ = 3.47 (d, J = 9.3 Hz, 1H), δ = 6.8 (td,

DOI: 10.1021/am506984m
ACS Appl. Mater. Interfaces 2015, 7, 4019−4028

J = 7.2 Hz, J = 0.9 Hz, 1H), δ = 6.71 (d, J = 3 Hz, 1H), δ = 6.58 (t, J = 7.2 Hz, 1H), δ = 5.87 (d, J = 6.1 Hz, 1H), δ = 3.89 (s, 3H); FT-IR (KBr, cm^{-1}) 3057, 3029, 2929, 2833, 1624, 1583, 1531, 1490, 1468, 1325, 1271, 1215, 1159, 829, 753, 698. Anal. Calcd for $C_{43}H_{33}N_3OPd$ (730.16 g/mol): C, 70.73; H, 4.56; N, 5.75. Found: C, 70.25; H, 4.55; N, 6.01.

Synthesis of **3**. Intermediate binuclear complex **A** (100 mg, 0.156 mmol) and 2 equiv of $H(O\wedge N)^3$ (155 mg, 0.312 mmol) were used.

3: orange solid; yield 94% (222 mg); mp 236 °C (amorphous on cooling); T_{dec} = 265 °C; ^{1}H NMR (300 MHz, $CDCl_3$, 25 °C, TMS) δ = 9.28 (d, J = 1 Hz, 1H), δ = 8.09 (s, 1H), δ = 7.82 (td, J = 8.1 Hz, J = 1.5 Hz, 1H), δ = 7.63 (d, J = 7.7 Hz, 1H), δ = 7.58 (d, J = 8.8 Hz, 2H), δ = 7.48 (d, J = 8.8 Hz, 2H), δ = 7.38 (t, J = 8.8 Hz, 3H), δ = 7.29−7.24 (m, 2H), δ = 7.12 (dd, J = 9.9 Hz, J = 1.1 Hz, 5H), δ = 7.07−7.03 (m, 8H), δ = 6.96 (d, J = 9.0 Hz, 2H), δ = 6.87 (t, J = 7.4 Hz, 1H), δ = 6.69 (d, J = 2.9 Hz, 1H), δ = 6.61 (t, J = 8.1 Hz, 1H), δ = 5.96 (dd, J = 8.1 Hz, J = 1.1 Hz, 1H), δ = 3.77 (s, 3H); FT-IR (KBr, cm^{-1}) 3024, 2931, 2815, 1622, 1587, 1526, 1508, 1490, 1462, 1415, 1385, 1324, 1280, 1215, 1158, 1025, 964, 831, 751, 696. Anal. Calcd for $C_{45}H_{35}N_3O_2Pd$ (756.2 g/mol): C, 71.47; H, 4.67; N, 5.56. Found: C, 71.50; H, 4.70; N, 5.61.

Synthesis of **4**. Intermediate mononuclear complex **B** (150 mg, 0.332 mmol), 1 equiv of $H(O\wedge N)^1$ (131 mg, 0.332 mmol), and 8 equiv of Na_2CO_3 (281 mg, 2.656 mmol) were solubilized in ca. 50 mL of 2-ethoxyethanol. The reaction mixture was stirred at 80 °C overnight to give a yellow precipitated. The solid was filtered off, washed with ethano,l and dried under vacuum. Recrystallization was performed in dichloromethane/ethanol solution.

4: orange solid; yield 79% (195 mg); mp 242 °C (amorphous on cooling); T_{dec} = 260 °C; ^{1}H NMR (300 MHz, $CDCl_3$, 25 °C, TMS) δ = 6.53 (dd, JPt = 43 Hz, J = 5.9 Hz, 1H), δ = 8.23 (s, 1H), δ = 7.99 (td, J = 8.4 Hz, J = 1.5 Hz, 1H), δ = 7.63 (d, J = 8.0 Hz, 1H), δ = 7.49 (d, J = 4.4 Hz, 2H), δ = 7.42 (d, J = 6.6 Hz, 1H), δ = 7.3−7.2 (m, 3H), δ = 7.16−6.97 (m, 13H), δ = 6.84 (t, J = 6.6 Hz, 1H), δ = 6.74 (d, J = 3.3 Hz, 1H), δ = 6.02 (d, J = 6.2 Hz, 1H), δ = 3.43 (s, 3H); FT-IR (KBr, cm^{-1}) 3079, 3027, 2934, 1623, 1607, 1586, 1495, 1467, 1384, 1316, 1267, 1215, 1157, 756, 695. Anal. Calcd for $C_{37}H_{29}N_3O_2Pt$ (742.72 g/mol): C, 59.83; H, 3.94; N, 5.66. Found: C, 59.90; H, 4.00; N, 5.71.

Synthesis of **5**. Intermediate mononuclear complex **B** (150 mg, 0.332 mmol), 1 equiv of $H(O\wedge N)^2$ (156 mg, 0.332 mmol), and 8 equiv of Na_2CO_3 (281 mg, 2.656 mmol) were used.

5: orange solid; yield 65% (178 mg); mp 270−271 °C (amorphous on cooling); T_{dec} = 280 °C; ^{1}H NMR (300 MHz, $CDCl_3$, 25 °C, TMS) δ = 9.53 (dd, JPt = 45 Hz, J = 8 Hz, 1H), δ = 8.22 (s, 1H), δ = 7.80 (t, J = 7.8 Hz, 1H), δ = 7.62 (q, J = 6 Hz, 4H), δ = 7.47 (d, J = 8 Hz, 2H), δ = 7.3−7.1 (m, 15H), δ = 7.1−7.0 (m, 2H), δ = 6.85 (t, J = 5.7 Hz, 1H), δ = 6.75 (d, J = 1.5 Hz, 1H), δ = 6.55 (t, J = 5 Hz, 1H), δ = 5.85 (dd, JPt = 45 Hz, J = 8.1 Hz, 1H); FT-IR (KBr, cm^{-1}) 3056, 3031, 2928, 1625, 1607, 1584, 1534, 1490, 1471, 1384, 1323, 1271, 1216, 1164, 1041, 82, 754, 698. Anal. Calcd for $C_{43}H_{33}N_3O_2Pt$ (818.82 g/mol): C, 63.07; H, 4.06; N, 5.13. Found: C, 63.10; H, 4.10; N, 5.25.

Synthesis of **6**. Intermediate mononuclear complex **B** (150 mg, 0.332 mmol), 1 equiv of $H(O\wedge N)^3$ (165 mg, 0.332 mmol), and 8 equiv of Na_2CO_3 (281 mg, 2.656 mmol) were used.

6: orange solid; yield 79% (214 mg); mp 263 °C (amorphous on cooling); T_{dec} = 280 °C; ^{1}H NMR (300 MHz, $CDCl_3$, 25 °C, TMS) δ = 9.53 (dd, JPt = 45 Hz, J = 5.5 Hz, 1H), δ = 8.21 (s, 1H), δ = 7.80 (t, J = 1.5 Hz, 1H), δ = 7.63−7.57 (m, 3H), δ = 7.63 (d, J = 8.8 Hz, 2H), δ = 7.39 (t, J = 8.4 Hz, 3H), δ = 7.1−7.2 (m, 3H), δ = 7.16−7.02 (m, 13H), δ = 6.83 (t, J = 7.3 Hz, 1H), δ = 6.74 (d, J = 3.3 Hz, 1H), δ = 6.62 (t, J = 7.3 Hz, 1H), δ = 6.74 (d, J = 3.3 Hz, 1H), δ = 6.62 (t, J = 6.2 Hz, 1H), δ = 5.87 (dd, JPt = 45 Hz, J = 8.4 Hz, 1H), δ = 3.75 (s, 3H); FT-IR (KBr, cm^{-1}): 3025, 2931, 2844, 1607, 1587, 1530, 1507, 1491, 1472, 1463, 1415, 1384, 1320, 1269, 1218, 1162, 1024, 831, 752, 696. Anal. Calcd for $C_{45}H_{35}N_3O_2Pt$ (844.86 g/mol): C, 63.97; H, 4.18; N, 4.97. Found: C, 64.00; H, 4.20; N, 5.00.

■ ASSOCIATED CONTENT

Supporting Information

Materials and methods, detailed synthesis of Schiff bases, supplementary cyclic voltammograms of modified Pt electrodes, and additional information on crystal structures, thermal behavior (DSC/TGA), and absorption spectra of complexes. This material is available free of charge via the Internet at http://pubs.acs.org.

■ AUTHOR INFORMATION

Corresponding Author

*Tel.: +390984492881. Fax: +390984492066. E-mail: nicolas.godbert@unical.it.

Notes

The authors declare no competing financial interest.

■ ACKNOWLEDGMENTS

This work was supported by the European Community's Seventh Framework Program (FP7 2007-2013), through MATERIA project (PONa3_00370) and MATELIOS (PON03PE_00092). We are highly grateful to Dr. Maria Penelope De Santo (Dipartimento di Fisica, Università della Calabria, Italia) for the AFM characterizations.

■ REFERENCES

(1) Forrest, S. R. The Path to Ubiquitous and Low-Cost Organic Electronic Appliances on Plastic. *Nature* **2004**, *428*, 911−918.

(2) Umeyama, T.; Imahori, H. Design and Control of Organic Semiconductors and their Nanostructures for Polymer-Fullerene-Based Photovoltaic Devices. *J. Mater. Chem. A* **2014**, *2*, 11545−11560.

(3) Sirringhaus, H. 25th Anniversary Article: Organic Field-Effect Transistors: The Path Beyond Amorphous Silicon. *Adv. Mater.* **2014**, *26*, 1319−1335.

(4) Scaccabarozzi, A. D.; Stingelin, N. Semiconducting: Insulating Polymer Blends for Optoelectronic Applications-A Review of Recent Advances. *J. Mater. Chem. A* **2014**, *2*, 10818−10824.

(5) Rivnay, J.; Owens, R. M.; Malliaras, G. G. The Rise of Organic Bioelectronics. *Chem. Mater.* **2014**, *26*, 679−685.

(6) Special Issue: Organic Electronics. *Adv. Mater.* **2013**, *25*, 1805−1954.

(7) Weiss, D.; Abkowitz, M. Advances in Organic Photoconductor Technology. *Chem. Rev.* **2010**, *110*, 479−526.

(8) Im, C.; Emelianova, E. V.; Bassler, H.; Spreitzer, H.; Beker, H. Intrinsic and Extrinsic Charge Carrier Photogeneration in Phenyl-Substituted Polyphenylenevinylene-Trinitrofluorenone Blend Systems. *J. Chem. Phys.* **2002**, *117*, 2961−2967.

(9) Cazati, T.; Santos, L. F.; Reis, F. T.; Faria, R. M. Efficiency of Extrinsic and Intrinsic Charge-Carrier Photogeneration Processes Obtained from the Steady-State Photocurrent Action Spectra of Poly(p-phenylene vinylene) Derivatives. *Appl. Phys. A: Mater. Sci. Process.* **2012**, *108*, 545−550.

(10) Camaioni, N.; Po, R. Pushing the Envelope of the Intrinsic Limitation of Organic Solar Cells. *J. Phys. Chem. Lett.* **2013**, *4*, 1821−1828.

(11) Nayak, P. K.; Bisquert, J.; Cahen, D. Assessing Possibilities and Limits for Solar Cells. *Adv. Mater.* **2011**, *23*, 2870−2876.

(12) Ghedini, M.; Aiello, I.; Crispini, A.; Golemme, A.; La Deda, M.; Pucci, D. Azobenzenes and Heteroaromatic Nitrogen Cyclopalladated Complexes for Advanced Applications. *Coord. Chem. Rev.* **2006**, *250*, 1373−1390.

(13) Ghedini, M.; Golemme, A.; Aiello, I.; Godbert, N.; Termine, R.; Crispini, A.; La Deda, M.; Lelj, F.; Amati, M.; Belviso, S. Liaisons Between Photoconductivity and Molecular Frame in Organometallic Pd(II) and Pt(II) Complexes. *J. Mater. Chem.* **2011**, *21*, 13434−13444.

(14) Godbert, N.; Dattilo, D.; Termine, R.; Aiello, I.; Bellusci, A.; Crispini, A.; Golemme, A.; Ghedini, M. UV/Vis to NIR Photo-

DOI: 10.1021/am506984m
ACS Appl. Mater. Interfaces 2015, 7, 4019−4028

conduction in Cyclopalladated Complexes. *Chem.—Asian J.* **2009**, *4*, 1141−1146.
(15) Ionescu, A.; Godbert, N.; Crispini, A.; Termine, R.; Golemme, A.; Ghedini, M. Photoconductive Nile Red Cyclopalladated Metallomesogens. *J. Mater. Chem.* **2012**, *22*, 23617−23626.
(16) Aiello, I.; Dattilo, D.; Ghedini, M.; Bruno, A.; Termine, R.; Golemme, A. Cyclopalladated Complexes as Photorefractive Materials with High Refractive Index Modulation. *Adv. Mater.* **2002**, *14*, 1233−1236.
(17) Aiello, I.; Dattilo, D.; Ghedini, M.; Golemme, A. Cyclometalated Complexes: A New Class of Highly Efficient Photorefractive Materials. *J. Am. Chem. Soc.* **2001**, *123*, 5598−5599.
(18) Termine, R.; Dattilo, D.; Aiello, I.; Ghedini, M.; Golemme, A. Photorefractive Performance Enhancement in Polymer Dispersions of Nanosized Crystalline Domains. *Adv. Mater.* **2003**, *15*, 723−726.
(19) Zhong, Y.-W.; Yao, C.-J.; Nie, H.-J. Electropolymerized Films of Vinyl-Substituted Polypyridine Complexes: Synthesis, Characterization, and Applications. *Coord. Chem. Rev.* **2013**, *257*, 1357−1372.
(20) Abruna, H. D.; Denisevich, P.; Umana, M.; Meyer, T. J.; Murray, R. W. Rectifying Interfaces Using Two-Layer Films of Electrochemically Polymerized Vinylpyridine and Vinylbipyridine Complexes of Ruthenium and Iron on Electrodes. *J. Am. Chem. Soc.* **1981**, *103*, 1−5.
(21) Hjelm, J.; Handel, R. W.; Hagfeldt, A.; Constable, E. C.; Housecroft, C. E.; Forster, R. J. Conducting Polymers Containing In-Chain Metal Centers: Electropolymerization of Oligothienyl-Substituted {M(tpy)2} Complexes and in Situ Conductivity Studies, M = Os(II), Ru(II). *Inorg. Chem.* **2005**, *44*, 1073−1081.
(22) Chen, X.-Y.; Yang, X.; Holliday, B. J. Photoluminescent Europium-Containing Inner Sphere Conducting Metallopolymer. *J. Am. Chem. Soc.* **2008**, *130*, 1546−1547.
(23) Kingsborough, R. P.; Swager, T. M. Electroactivity Enhancement by Redox Matching in Cobalt Salen-Based Conducting Polymers. *Adv. Mater.* **1998**, *10*, 1100−1104.
(24) Kingsborough, R. P.; Swager, T. M. Polythiophene Hybrids of Transition-Metal Bis(salicylidenimine)s: Correlation between Structure and Electronic Properties. *J. Am. Chem. Soc.* **1999**, *121*, 8825−8834.
(25) Foster, K.; McCormac, T. Synthesis, Characterization and Electrochemical Polymerization of a Ru^{2+} Functionalized Pyrrole Monomer. *Electroanalysis* **2007**, *19*, 1509−1517.
(26) Ellis, C. D.; Margerum, L. D.; Murray, R. W.; Meyer, T. J. Oxidative Electropolymerization of Polypyridyl Complexes of Ruthenium. *Inorg. Chem.* **1983**, *22*, 1283−1291.
(27) Brown, K. L.; Mottola, H. A. Voltammetric, Chronocoulometric, and Spectroelectrochemical Studies of Electropolymerized Films Based on Cu(II/I)−4,9,16,23-Tetraaminophthalocyanine. *Langmuir* **1998**, *14*, 3411−3417.
(28) Venkatanarayanan, A.; Sephar-Deleze, A. M.; Dennany, L.; Pellegrin, Y.; Keyes, T. E.; Forster, R. J. Ruthenium Aminophenanthroline Metallopolymer Films Electropolymerized from an Ionic Liquid: Deposition and Electrochemical and Photonic Properties. *Langmuir* **2008**, *24*, 11233−11238.
(29) Yen, H. J.; Liou, G.-S. Solution-Processable Triarylamine-Based Electroactive High Performance Polymers for Anodically Electrochromic Applications. *Polym. Chem.* **2012**, *3*, 255−264.
(30) Leung, M. K.; Chou, M.-Y.; Su, Y. O.; Chiang, C. L.; Chen, H. L.; Yang, C. F.; Yang, C. C.; Lin, C. C.; Chen, H.-T. Diphenylamino Group as an Effective Handle to Conjugated Donor−Acceptor Polymers through Electropolymerization. *Org. Lett.* **2003**, *5*, 839−842.
(31) Qiu, D.; Zhao, Q.; Bao, X.; Liu, K.; Wang, H.; Guo, Y.; Zhang, L.; Zeng, J.; Wang, H. Electropolymerization and Characterization of an Alternatively Conjugated Donor−Acceptor Metallopolymer: Poly-$[Ru(4'-(4-(Diphenylamino)phenyl)-2,2':6',2''-Terpyridine)2]^{2+}$. *Inorg. Chem. Commun.* **2011**, *14*, 296−299.
(32) Qiu, D.; Bao, X.; Zhao, Q.; Feng, Y.; Wang, H.; Liu, K. Electrochromic and Proton-Induced Phosphorescence Properties of Pt(II) Chlorides with Arylamine Functionalized Cyclometalating Ligands. *J. Mater. Chem. C* **2013**, *1*, 695−704.
(33) Cocherel, N.; Leriche, P.; Ripaud, E.; Gallego-Planas, N.; Frère, P.; Roncali, J. Electropolymerization of Triphenylamine-Dithiafulvene Hybrid Extended pi-Conjugated Systems. *New J. Chem.* **2009**, *33*, 801−806.
(34) Iwan, A.; Sek, D. Polymers with Triphenylamine Units: Photonic and Electroactive. *Prog. Polym. Sci.* **2011**, *36*, 1277−1325.
(35) Constable, E. C.; Thompson, A. M. W. C.; Leese, T. A.; Reese, D. G. F.; Tocher, D. Cyclometallation Reactions of 2-phenylpyridine; Crystal and Molecular structure of (2-{2-pyridyl} phenyl)palladium-(II) Tetramer and (2-{2-pyridyl} phenyl)mercury(II) Tetramer. *Inorg. Chim. Acta* **1991**, *182*, 93−100.
(36) Godbert, N.; Pugliese, T.; Aiello, I.; Bellusci, A.; Crispini, A.; Ghedini, M. Efficient, Ultrafast, Microwave-Assisted Syntheses of Cycloplatinated Complexes. *Eur. J. Inorg. Chem.* **2007**, 5105−5111.
(37) Larumbe, D.; Gallardo, I.; Andrieux, C. P. Anodic Oxidation of Some Tertiary Amines. *J. Electroanal. Chem.* **1991**, *304*, 241−247.
(38) Brown, K. L.; Gray, S. B. Cyclic Voltammetric Studies of Electropolymerized Films Based on Ruthenium(II/III) Bis(1,10 phenanthroline) (4-methyl-4′vinyl-2,2′-bipyridine). *Int. J. Chem. (Toronto, ON, Can.)* **2010**, *2*, 3−9.
(39) Lana-Villareal, T.; Campina, J. M.; Guijarro, N.; Gomez, R. Solid-State Electropolymerization and Doping of Triphenylamine as a Route for Electroactive Thin Films. *Phys. Chem. Chem. Phys.* **2011**, *13*, 4013−4021.
(40) Bässler, H. Charge Transport in Disordered Organic Photoconductors a Monte Carlo Simulation Study. *Phys. Status Solidi B* **1993**, *175*, 15−56.
(41) Onsager, L. Deviations from Ohm's Law in Weak Electrolytes. *J. Chem. Phys.* **1934**, *2*, 599−615.
(42) Shah, A. *Thin Film Silicon Solar Cells*; EPFL Press: Lausanne, Switzerland, 2010; pp 58−61.
(43) Pal, R. K.; Yadav, S.; Aghinotri, A. K.; Kumar, D.; Kumar, A. Composition Dependence of Photoconductivity in Amorphous Se70Te30-xZnx Thin Films. *J. Non-Oxide Glasses* **2009**, *1*, 285−291.
(44) Hendrickx, E.; Zhang, Y.; Ferrio, K. B.; Herlocker, J. A.; Anderson, J.; Armstrong, N. R.; Mash, E. A.; Persoons, E. A. P.; Peyghambarian, N.; Kippelen, B. Photoconductive Properties of PVK-based Photorefractive Polymer Composites Doped with Fluorinated Styrene Chromophores. *J. Mater. Chem.* **1999**, *9*, 2251−2258.
(45) Quintana, J. A.; Villalvilla, J. M.; Boj, P. G.; Martìn-Gomis, L.; Ortiz, J.; Fernàndez-Làzaro, F.; Sastre-Santos, A.; Dìaz Garcìa, M. A. Enhanced Photorefractivity of Poly(N-vinylcarbazole)-Based Composites through Electric-Field Treatments and Ionic Liquid Doping. *Adv. Funct. Mater.* **2009**, *19*, 428−437.
(46) Tong, M.; Cho, S.; Rogers, J. T.; Schmidt, K.; Hsu, B. B. Y.; Moses, D.; Coffin, R. C.; Kramer, E. J.; Bazan, G. C.; Heeger, A. J. Higher Molecular Weight Leads to Improved Photoresponsivity, Charge Transport and Interfacial Ordering in a Narrow Bandgap Semiconducting Polymer. *Adv. Funct. Mater.* **2010**, *20*, 3959−3965.
(47) Hernandez-Sosa, G.; Coates, N. E.; Valouch, S.; Moses, D. High Photoconductive Responsivity in Solution-Processed Polycrystalline Organic Composite Films. *Adv. Funct. Mater.* **2011**, *21*, 927−931.
(48) Pommerehne, J.; Vestweber, H.; Guss, W.; Mahrt, R. F.; Bässler, H.; Porsch, M.; Daub, J. Efficient Two Layer Leds on a Polymer Blend Basis. *Adv. Mater.* **1995**, *7*, 551−554.
(49) *SAINT, Version 6.45*; Bruker Analytical X-ray Systems Inc.: WI, 2003.
(50) *SHELXTL-NT, Version 5.1*; Bruker Analytical X-ray Systems Inc.: WI, 1999.
(51) Brandeburg, K.; Putz, H. *DIAMOND 3.1b, Crystal Impact GbR, CRYSTAL IMPACT*; GBR: Bonn, Germany, 2006.

DOI: 10.1021/am506984m
ACS Appl. Mater. Interfaces 2015, 7, 4019−4028